Potsdam Institute for Climate Impact Research

P I K

# Early warning of noise-induced catastrophic high-amplitude oscillations in an airfoil model

Jinzhong Ma, Qi Liu, Yong Xu, Jürgen Kurths

**Document Version**
Version of Record (Publisher Version)

This version is available at
https://publications.pik-potsdam.de/pubman/item/item_27031

**Originally published as**
Ma, J., Liu, Q., Xu, Y., Kurths, J. (2022): Early warning of noise-induced catastrophic high-amplitude oscillations in an airfoil model. - Chaos, 32, 3, 033119.
https://doi.org/10.1063/5.0084796

**Terms of Use**
This article may be downloaded for personal use only. Any other use requires prior permission of the author and AIP Publishing.

Chaos
An Interdisciplinary Journal of Nonlinear Science

RESEARCH ARTICLE | MARCH 17 2022

# Early warning of noise-induced catastrophic high-amplitude oscillations in an airfoil model

Jinzhong Ma; Qi Liu; Yong Xu ; Jürgen Kurths

Check for updates

*Chaos* 32, 033119 (2022)
https://doi.org/10.1063/5.0084796

View Online
Export Citation

**Articles You May Be Interested In**

Complex nonlinear dynamics and vibration suppression of conceptual airfoil models: A state-of-the-art overview

*Chaos* (June 2022)

Preloaded freeplay wide-bandwidth low-frequency piezoelectric harvesters

*Appl. Phys. Lett.* (July 2015)

Early warning of noise-induced critical transitions in two-dimensional ecosystems

*Chaos* (February 2026)

01 April 2026 12:40:30


AIP Publishing

# Early warning of noise-induced catastrophic high-amplitude oscillations in an airfoil model

Cite as: Chaos **32**, 033119 (2022); doi: 10.1063/5.0084796
Submitted: 10 January 2022 · Accepted: 1 March 2022 ·
Published Online: 17 March 2022

View Online Export Citation CrossMark

Jinzhong Ma,[1] Qi Liu,[2] Yong Xu,[2,3,a)] and Jürgen Kurths[4,5]

## AFFILIATIONS

[1]School of Mathematical Sciences, Shanxi University, Taiyuan 030006, China
[2]School of Mathematics and Statistics, Northwestern Polytechnical University, Xi'an 710072, China
[3]MIIT Key Laboratory of Dynamics and Control of Complex Systems, Northwestern Polytechnical University, Xi'an 710072, China
[4]Potsdam Institute for Climate Impact Research, Potsdam 14412, Germany
[5]Department of Physics, Humboldt University at Berlin, Berlin 12489, Germany

[a)]**Author to whom correspondence should be addressed:** hsux3@nwpu.edu.cn

## ABSTRACT

Noise-induced tipping from a low-amplitude oscillation state to a high-amplitude one is widespread in airfoil systems. Its occurrence may cause fatigue damage to the wing structure of an aircraft, which directly threatens its flight safety. Therefore, it is of utmost importance to predict the occurrence of noise-induced high-amplitude oscillations as the system parameters vary in airfoil systems. Taking a two-degrees-of-freedom airfoil model with random loadings as a prototype class of real systems, the prediction of noise-induced tipping from low-amplitude to high-amplitude oscillations is carried out in the present study. First, we analyze the effects of random fluctuations on the system response. The results show that noise-induced catastrophic high-amplitude oscillations take place before the bifurcation point of the corresponding deterministic airfoil model. Subsequently, the possibility that the low-amplitude oscillation state of the given noisy model jumps to the high-amplitude one is analyzed based on the escape probability. Then, the new concept of the high-risk region is defined. This is an efficient early warning indicator to approximately quantify the ranges of the system parameters where noise-induced high-amplitude oscillations may occur. Compared with the existing early warning indicators, this method is a non-local universal concept of stability. More importantly, it may provide theoretical guidance for aircraft designers to take some measures to avoid such catastrophic critical jump phenomena in practical engineering applications.

*Published under an exclusive license by AIP Publishing.* https://doi.org/10.1063/5.0084796

01 April 2026 12:40:30

**Random fluctuations in a flight environment can induce tipping from a low-amplitude oscillation state to a high-amplitude one of an airfoil system. These typically undesirable high-amplitude oscillations often lead to airfoil structural damage, thereby increasing the risk of flight safety issues such as the aircraft breaking up in mid-air. Therefore, early warning of high-amplitude oscillations under random fluctuations has been a major problem faced during the safe flight of the aircraft. Many studies, in recent years, have been devoted to exploring early warning indicators to predict and characterize the onset of high-amplitude oscillations. However, these existing indicators can only warn of high-amplitude oscillations that are impending, which leaves operators not having enough time to avoid the occurrence of these catastrophic events. To overcome these problems, in this paper, we introduce a new and non-local concept: *the high-risk region*. It can provide early warning signals for the airfoil structure by quantifying the ranges of the system parameters where noise-induced high-amplitude oscillations may occur in advance.**

## I. INTRODUCTION

Many engineering systems exhibit tipping points where small random fluctuations spark a sudden transition to a catastrophic high-amplitude oscillation state.[1,2] One example of such engineering systems is the airfoil aeroelastic system. In practical aircraft design, the high-amplitude oscillation phenomena are not rare and highly undesirable.[3–10] At times, they can severely jeopardize the performance and even lead to a possible great disaster. Thus, early warning of the high-amplitude oscillations in an airfoil system has been an active area of research.


Published under an exclusive license by AIP Publishing

In general, the nonlinear factors in airfoil models can induce very rich dynamic behaviors. Coupling of nonlinearity and random loadings makes the dynamics even more complex.[11–13] Despite this, uncertain influences should be taken into account in the exploration of aircraft structures. This is of high practical significance and may provide valuable information to an efficient and safe design of the aircraft wings.[14–17]

During the past few years, many investigations have been devoted to exploring dynamic responses of the airfoil model with random excitations.[18–21] For instance, turbulence suffered by a two-degrees-of-freedom airfoil (TDOFA) system in the vertical direction was modulated as an additive white noise, and the saddle-node and subcritical bifurcation associated with the proposed random airfoil model were investigated.[22] Several early warning indicators, including multi-fractality, entropy measures, Lempel–Ziv complexity, and Hurst exponents, were proposed to capture changes of the dynamic responses in random airfoil aeroelastic system systems.[23–25] It should be noted here that these indicators can only warn impending catastrophic dynamic responses. However, it is already difficult for operators to prevent the occurrence of these catastrophic events at this time. In addition, a number of works focused on airfoil models subjected to narrow-band random excitations, which have been shown to exist in several aeroelastic problems of a wing.[26–34] Specifically, the power spectrum density of the airfoil instability tonal noise has been proved experimentally to have a narrow-band characteristic.[35] Stochastic jumps from low-amplitude to high-amplitude oscillations of a TDOFA model with Gaussian or narrow-band noise excitations were studied, which decrease the performance of an aircraft and could even lead to a catastrophe in flight.[36] All these existing results provide ideas for us to further establish a more general early warning indicator of high-amplitude oscillations in an additive narrow-band random excitation-induced airfoil model.

In fact, the occurrence of noise-induced tipping from low-amplitude to high-amplitude oscillations depends on the stability of the low-amplitude oscillation state against random perturbations. To overcome the limitation that the existing indicators can only provide early warning signals when catastrophic dynamic responses are imminent, an earlier analysis of non-local stability is necessary. In Refs. 37–39, we have proposed a non-local and nonlinear early warning indicator, the parameter dependent basin of the unsafe regime. This tool can successfully quantify the ranges of the parameters where Gaussian white noise or Lévy noise-induced critical transitions may occur in multi-stable systems. Based on these results, in this study, a new concept of the high-risk region is introduced to warn noise-induced catastrophic high-amplitude oscillations in the airfoil model.

The remainder of this paper is arranged as follows: In Sec. II, the TDOFA model subject to a narrow-band noise is introduced. In Sec. III, the approximate analytical solutions of the amplitude–frequency responses obtained by the multiple-scale method are compared with the results from numerical simulations. Furthermore, noise-induced high-amplitude oscillations that take place earlier are uncovered. Section IV introduces the new concept of the high-risk region to quantify the parameters, where noise-induced high-amplitude oscillations may occur. Finally, conclusions are presented in Sec. V.

## II. TDOFA MODEL WITH RANDOM LOADING

In this section, a conceptual TDOFA model oscillating in pitch and plunge is introduced. Figure 1 shows a typical TDOFA section containing various symbols used in the TDOFA model.[4,36] Among them, $\alpha$ denotes the pitch angle of the airfoil, which is positive if nose-up. $h$ represents the plunging deflection, and it is positive if it is downward. $U$ denotes the flow velocity, and $L$ and $M$ represent the aerodynamic force and moment acting on the airfoil, respectively. $G$ indicates the center of gravity, $F$ is the point of the force application, $b$ is the airfoil semi-chord, and $EA$ is the elastic axis. $ab$ is the distance of the elastic axis from the mid-chord, while the center of gravity is located at a distance $x_\alpha b$ from the elastic axis. Both distances are positive when measured toward the trailing edge of the airfoil.

Considering the steady aerodynamic force based on the introduction of the non-dimensional plunge deflection $\xi = h/b$ and the time $\tau = Ut/b$, a non-dimensional TDOFA model with an external random loading can be written as[4,8,9]

$$\begin{aligned} &\ddot{\xi} + x_\alpha \ddot{\alpha} + \zeta_\xi \dot{\xi} + (\omega_\xi/\omega_\alpha)^2(\xi + \beta_\xi \xi^3) = -2Q\alpha/\mu, \\ &\frac{x_\alpha}{r_\alpha{}^2}\ddot{\xi} + \ddot{\alpha} + \zeta_\alpha \dot{\alpha} + \alpha + \beta_\alpha \alpha^3 = (1+2a)Q\alpha/\mu r_\alpha{}^2 + \eta(\tau), \end{aligned} \tag{1}$$

where $r_\alpha$ is the radius of gyration, and $Q = (U/b\omega_\alpha)^2$ is called the generalized flow velocity. $\mu = m/\pi\rho b^2$ is the non-dimensional mass of the airfoil with the mass of the airfoil $m$ and the air density $\rho$. $\omega_\xi$ and $\omega_\alpha$ represent the uncoupled natural frequencies, $\beta_\xi$ and $\beta_\alpha$ stand for the nonlinear stiffness coefficients, and $\zeta_\xi$ and $\zeta_\alpha$ are the damping ratios, in both degrees of freedom, respectively. In particular, $\eta(\tau)$ is the random harmonic excitation used to characterize the random loading of the external environment, which is described as

$$\eta(\tau) = A\cos[\Omega\tau + \nu W(\tau)],$$

where $W(\tau)$ is a standard Wiener process, and $A$ denotes the amplitude of the random excitation with the central frequency $\Omega$. Moreover, $\nu \geq 0$, is the intensity of the stochastic excitation, which is assumed to be a small parameter in the present paper. Obviously, the random excitation $\eta(t)$ will degenerate into a deterministic periodic force when $\nu = 0$.

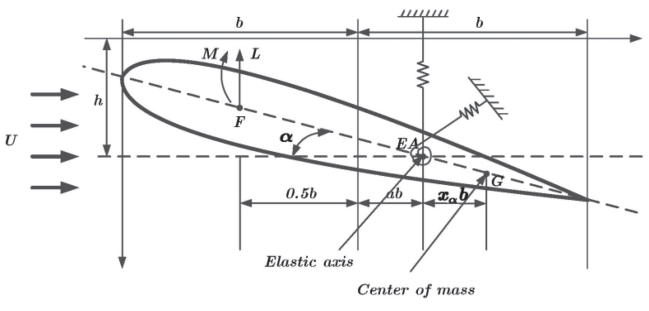


**FIG. 1.** Schematic of the TDOFA section model.[36]

01 April 2026 12:40:30


Published under an exclusive license by AIP Publishing

To enable a theoretical analysis, we assume that the coupling and nonlinearity terms in the airfoil model are very small. So, the scale transformation is introduced with a small parameter $0 < \varepsilon \ll 1$, and some parameters are renewed as

$$x_\alpha \to \varepsilon x_\alpha,\ \ \zeta_\xi \to \varepsilon\zeta_\xi,\ \ \zeta_\alpha \to \varepsilon\zeta_\alpha,\ \ \beta_\xi \to \varepsilon\beta_\xi,\ \ \beta_\alpha \to \varepsilon\beta_\alpha,$$
$$Q \to \varepsilon Q,\ \ A \to \varepsilon A.$$

Then, the airfoil system (1) becomes,

$$\begin{aligned} &\ddot{\xi} + \varepsilon x_\alpha \ddot{\alpha} + \varepsilon\zeta_\xi\dot{\xi} + {\omega_{10}}^2\xi + \varepsilon{\omega_{10}}^2\beta_\xi\xi^3 = -2\varepsilon Q\alpha/\mu, \\ &\varepsilon\frac{x_\alpha}{{r_\alpha}^2}\ddot{\xi} + \ddot{\alpha} + \varepsilon\zeta_\alpha\dot{\alpha} + {\omega_{20}}^2\alpha + \varepsilon\beta_\alpha\alpha^3 = \varepsilon A\cos[\Omega t + \nu W(\tau)], \end{aligned} \tag{2}$$

where $\omega_{10} = \omega_\xi/\omega_\alpha$ and $\omega_{20} = \sqrt{1-(1+2a)Q/\mu{r_\alpha}^2}$.

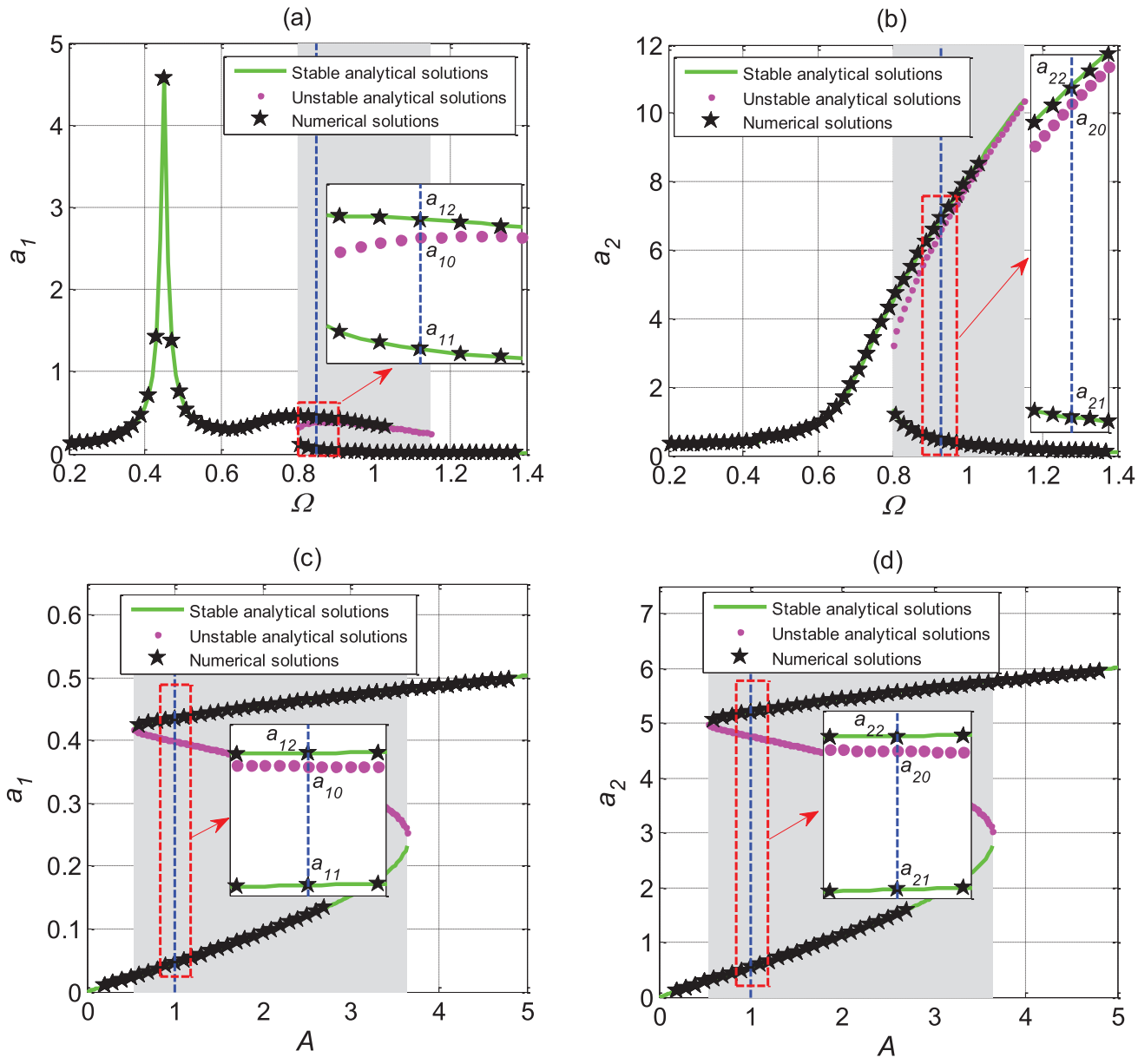


**FIG. 2.** The steady-state amplitude responses of system (2) with $\nu = 0$. (a) and (b) The amplitude–frequency responses of plunge and pitch motion ($A = 1.5$). (c) and (d) The plunge and pitch amplitudes as the external excitation amplitude $A$ vary ($\Omega = 0.84$). -, stable analytical solutions; ·, unstable analytical solutions; ★, numerical solutions.

01 April 2026 12:40:30


Published under an exclusive license by AIP Publishing

In what follows, a comparison of the steady-state amplitude–frequency response from the approximate analytical method and the numerical method is presented. The approximate analytical results by the multiple-scale method can be found in the Appendix. The numerical simulations of the original system (2) are carried out based on the classical fourth-order Runge–Kutta integral scheme with the time step $\Delta\tau = 0.01$. The values of system parameters are chosen as $\mu = 20$, $a = -0.1$, $x_\alpha = 0.25$, $r_\alpha{}^2 = 0.5$, $\omega_\xi/\omega_\alpha = \sqrt{0.2}$, $\zeta_\xi = \zeta_\alpha = 0.125$, $\beta_\xi = 0$, $\beta_\alpha = 0.1$, $\varepsilon = 0.1$, and $Q = 6.0$.[4,10,16,36] Moreover, in this process, the plunge amplitude $a_1(\tau)$ and the pitch amplitude $a_2(\tau)$ are calculated via $a_1 = \sqrt{x_1^2(\tau) + [\dot{x}_1(\tau)/\Omega]^2}$ and $a_2 = \sqrt{x_2^2(\tau) + [\dot{x}_2(\tau)/\Omega]^2}$, respectively.

Figure 2 shows the steady-state amplitude responses of the forced airfoil calculated through Eq. (A10) in the Appendix. Furthermore, the numerical solutions are obtained by the forward and backward scanning of frequency $\Omega$ or amplitude $A$ of the external periodic excitation of the original system (2). It is found that the results obtained by the multiple-scale method are consistent with the numerical results. More interestingly, as marked by the

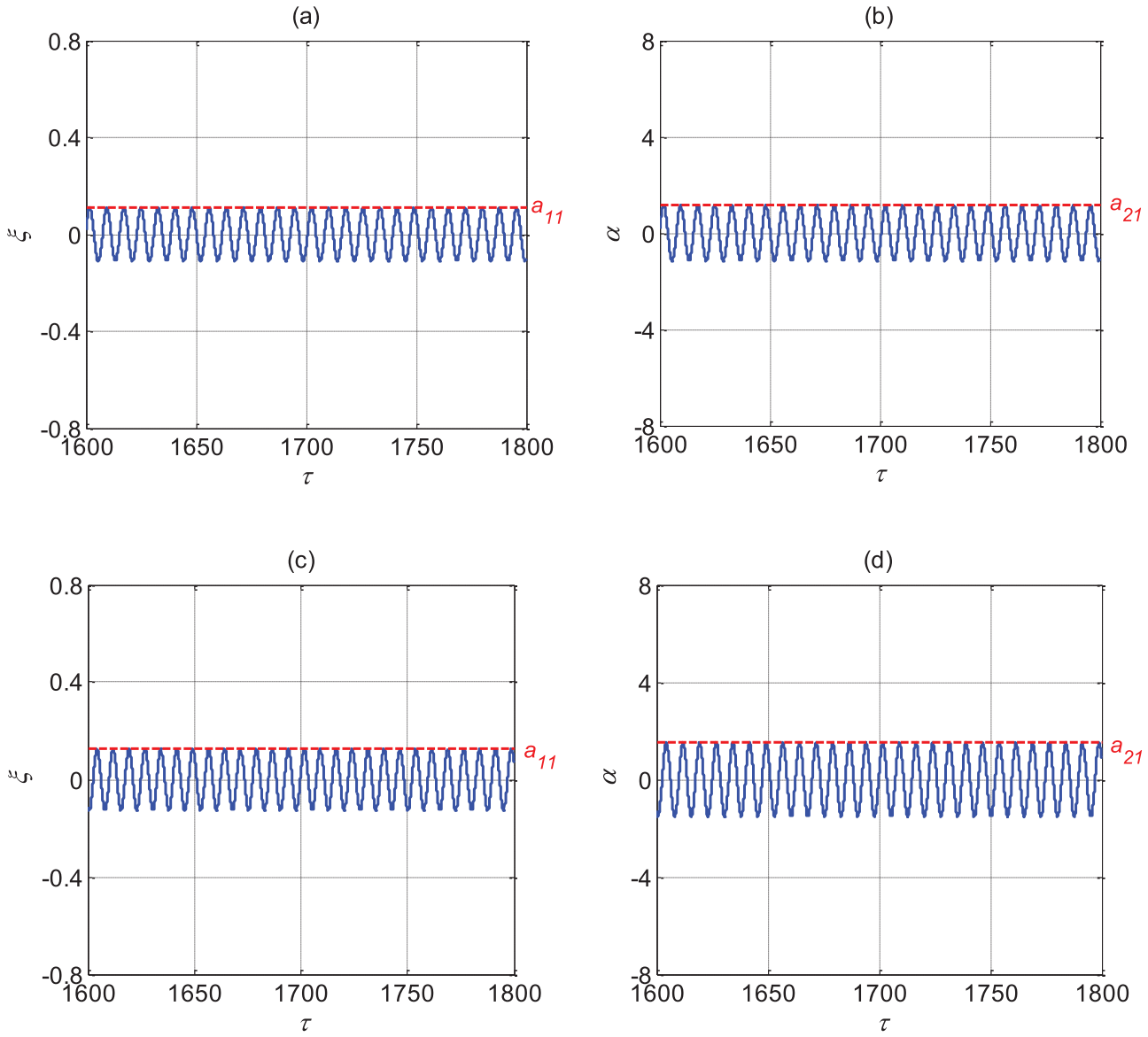


**FIG. 3.** The time histories of plunge and pitch motion with the same initial values $x_1(0) = x_2(0) = 0.1$, $\dot{x}_1(0) = \dot{x}_2(0) = 0.1$, and $\nu = 0$. (a) and (b) $A = 1.5$, $\Omega = 0.81$. (c) and (d) $A = 2.6$, $\Omega = 0.84$.

01 April 2026 12:40:30


Published under an exclusive license by AIP Publishing

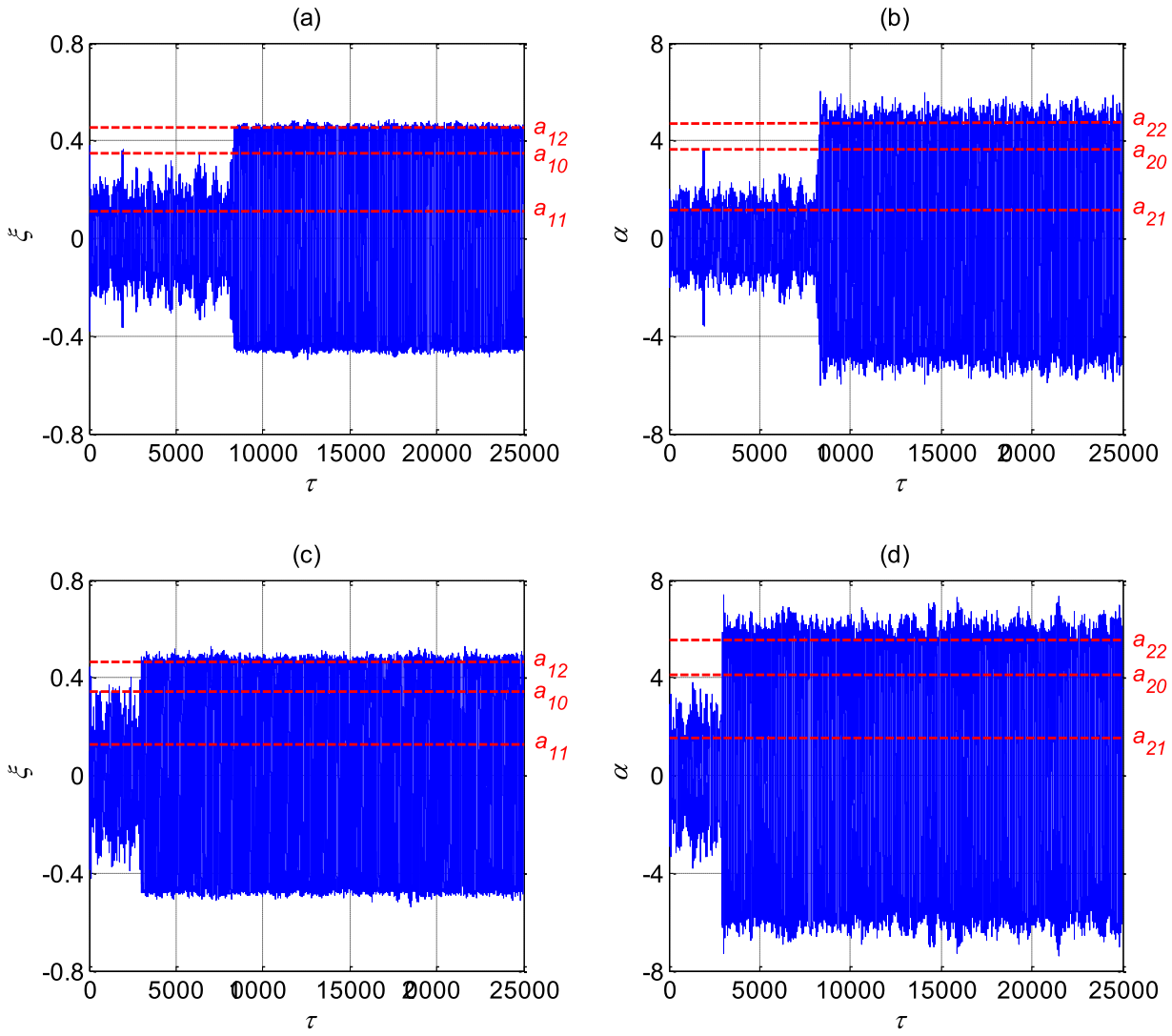


**FIG. 4.** The time histories of plunge and pitch motion with the same initial values $x_1(0) = x_2(0) = 0.1, \dot{x}_1(0) = \dot{x}_2(0) = 0.1$, and $\nu = 0.06$. (a) and (b) $A = 1.5, \Omega = 0.81$. (c) and (d) $A = 2.6, \Omega = 0.84$.

gray bistable regions, multiple-values response phenomena appear within a certain range of $\Omega$ or $A$ of the external excitation. As $\Omega$ decreases or $A$ increases, the tipping from the lower-branch to the upper-branch occurs, when passing through the bifurcation points. Correspondingly, the number of steady-state solutions changes from three to one. The three solutions such as $a_{11}$, $a_{10}$ and $a_{12}$ are shown in the enlarged local view in Fig. 2(a). Among them, $a_{11}$ and $a_{12}$ are two stable solutions, and $a_{10}$ is the unstable solution. Similar enlarged local views are also given in Figs. 2(b)–2(d). Although the bistable regions are different under the multiple-scale and numerical solutions, a part of consistency lays a solid foundation for us to directly adopt the numerical method to investigate noise-induced catastrophic high-amplitude oscillations in the following. In the numerical case, two probable steady-state responses coexist for $\Omega \in [0.80, 1.03]$ with the step $\Delta\Omega = 0.01$ or for $A \in [0.6, 2.7]$ with the step $\Delta A = 0.1$. Once the airfoil system crosses the bifurcation point $\Omega = 0.80$or$A = 2.7$, the catastrophic tipping from the low-amplitude oscillation state to the high-amplitude one will take place.

## III. NOISE-INDUCED HIGH-AMPLITUDE OSCILLATIONS

In this section, the effects of the noise on tipping from low-amplitude to high-amplitude oscillations will be investigated for the proposed stochastic TDOFA model.

01 April 2026 12:40:30


Published under an exclusive license by AIP Publishing

Before analyzing the influences of random fluctuations on the tipping, Figs. 3(a) and 3(b) first show the time histories of the plunge and pitch motion in the deterministic case with $\Omega = 0.81$. It is very close to the bifurcation point $\Omega = 0.80$. Similarly, the time histories of the plunge and pitch motion very close to the bifurcation point $A = 2.7$ are shown in Figs. 3(c) and 3(d). Here, the initial values are taken as $x_1(0) = x_2(0) = 0.1$, $\dot{x}_1(0) = \dot{x}_2(0) = 0.1$ to ensure that the initial state of system (2) converges to low-amplitude oscillations. Corresponding to Fig. 2(a), system (2) stays in a low-amplitude oscillation state with the response amplitude $a_{11}$ as shown in Fig. 3(a). Similarly, as given in Figs. 3(b)–3(d), system (2) is also in a low-amplitude oscillation state one-to-one corresponding to Figs. 2(b)–2(d). However, can random fluctuations induce catastrophic high-amplitude oscillations? Figure 4 answers this question very well. It is found that, under the same initial values as in Fig. 3, the noise-induced tipping from the low-amplitude oscillation state to the high-amplitude one occurs in the plunge and pitch motion with $\nu = 0.06$. As shown in Fig. 4(a), the response amplitude of the plunge motion crosses the barrier $a_{10}$ from $a_{11}$ to reach $a_{12}$. Similar results are found in Figs. 4(b)–4(d). All these results indicate that random fluctuations can induce catastrophic high-amplitude oscillations before $\Omega$ or $A$ reach their bifurcation points.

To further explore the high-amplitude oscillation state that takes place in advance under random fluctuations, the steady-state probability density functions (PDFs) of the response amplitudes of the pitch motion are calculated. In Fig. 5(a), it can be found that system (2) always stays in the low-amplitude oscillation state with the response amplitude $a_{21}$ when $\nu = 0$, which is consistent with the result in Fig. 3(d). On the contrary, in Fig. 5(b), the steady-state PDF $P_{st}(a_2)$ of pitch motion appears in unimodal form with most of the density concentrated around the response amplitude $a_{22}$ when $\nu = 0.06$. That is, system (2) is in a state of high-amplitude oscillations, which is basically consistent with the result in Fig. 4(d). Furthermore, these noise-induced similar dynamic behaviors can also be found in the steady-state PDFs of the response amplitudes of plunge motion due to the mutual coupling effect of both degrees of freedom.

In fact, random fluctuations in the flight environment of the aircraft can induce tipping from the low-amplitude oscillation state to the high-amplitude one in the airfoil system. Such catastrophic high-amplitude oscillations can cause fatigue damage to the wing structure, thereby increasing the risk of flight safety issues such as the aircraft breaking up in mid-air. Therefore, an early warning of noise-induced catastrophic high-amplitude oscillations in an airfoil system in advance can ensure the flight safety of the aircraft and reduce the risk of accidents. In the following, a more general, early warning indicator of noise-induced catastrophic high-amplitude oscillations will be established.

## IV. HIGH-RISK REGIONS OF NOISE-INDUCED HIGH-AMPLITUDE OSCILLATIONS

Since the response amplitude of the plunge or pitch motion has a transition or escape that crosses the corresponding unstable state, the noise-induced tipping from the low-amplitude oscillation state to the high-amplitude one occurs in system (2). Therefore, to determine whether system (2) with a low-amplitude oscillation in its initial state can exhibit high-amplitude oscillations under $\Omega \in [0.80,\ 1.03]$, $A \in [0.6, 2.7]$, and a given noise intensity $\nu$, it is necessary to first calculate the probability of system (2) crossing the unstable state. Here, a numerical method for calculating the escape probability is given as follows.

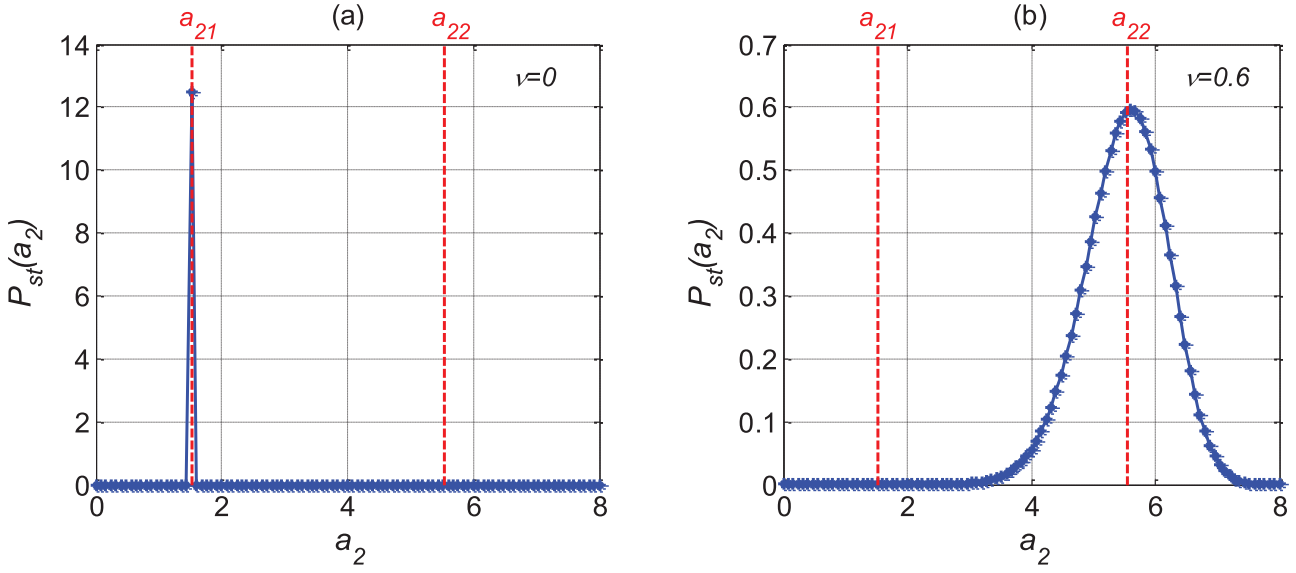


**FIG. 5.** The steady-state PDFs $P_{st}(a_2)$ of the pitch amplitude $a_2$ with $A = 2.6$, $\Omega = 0.84$, and the same initial values $x_1(0) = x_2(0) = 0.1$, $\dot{x}_1(0) = \dot{x}_2(0) = 0.1$. (a) $\nu = 0$. (b) $\nu = 0.06$.

01 April 2026 12:40:30


Published under an exclusive license by AIP Publishing

For $\Omega \in [0.80,\ 1.03]$, $A \in [0.6, 2.7]$, and a given noise intensity $v$, suppose that a certain time history of the plunge or pitch motion of system (2) without a transient state has $N$ local maxima, where $M$ of these $N$ values are greater than the corresponding unstable solution ($a_{10}$ or $a_{20}$ as shown in Fig. 2). Then, the ratio

$$M/N \triangleq P_E$$

is the escape probability of system (2) jumping from low-amplitude to high-amplitude oscillations.[40–44] It should be reminded that here, this time history is the average result of 10 000 trajectories.

Based on the numerical method introduced above, the escape probabilities of the plunge and pitch motion with varying $\Omega$ and $A$ under different noise intensities $v$ are presented in Fig. 6. In Figs. 6(a) and 6(b), it is found that, as $\Omega$ gradually decreases to the bifurcation point $\Omega = 0.80$, the escape probabilities gradually increase. In particular, the escape probabilities of the plunge and

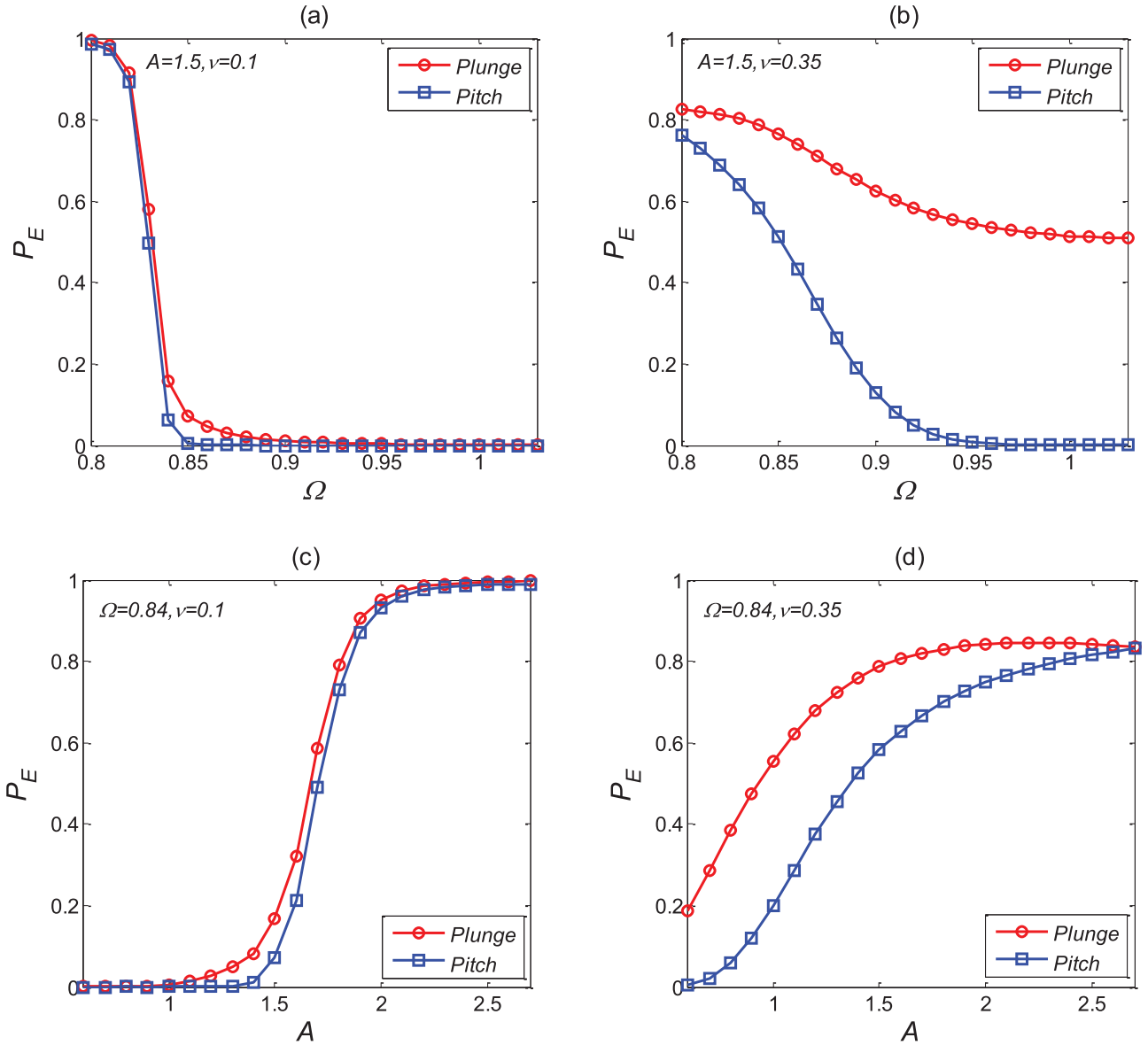


**FIG. 6.** The escape probabilities $P_E$ of plunge and pitch motion with different $v$. (a) and (b) $P_E$ of plunge and pitch motion against $\Omega$ ($A = 1.5$). (c) and (d) $P_E$ of the plunge and pitch motion as $A$ vary ($\Omega = 0.84$). The initial values are also taken as $x_1(0) = x_2(0) = 0.1$, $\dot{x}_1(0) = \dot{x}_2(0) = 0.1$ to ensure that the initial state of system (2) converges to the low-amplitude oscillation state.

01 April 2026 12:40:30


Published under an exclusive license by AIP Publishing

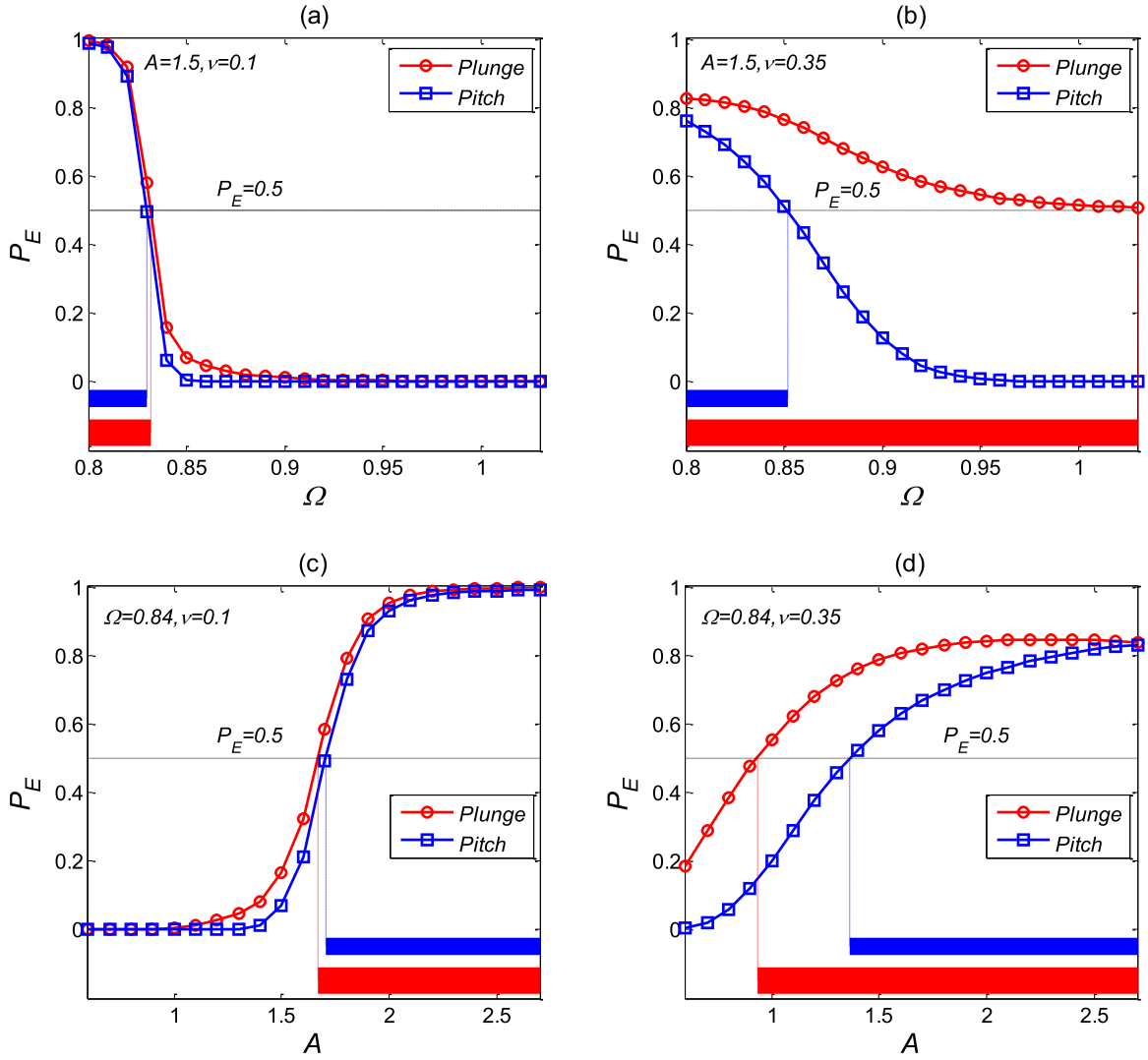


**FIG. 7.** The escape probabilities and the high-risk regions of plunge and pitch motion against Ω and $A$. (a) $A = 1.5$, $\nu = 0.1$. (b) $A = 1.5$, $\nu = 0.35$. (c) $\Omega = 0.84$, $\nu = 0.1$. (d) $\Omega = 0.84$, $\nu = 0.35$. The inserted horizontal dotted line is $P_E = 0.5$. The thick bar-type and thin bar-type represent the high-risk regions of plunge and pitch motion, respectively.

pitch motion almost reach 1 at $\Omega = 0.80$, when $\nu = 0.1$. Although the escape probabilities at $\Omega = 0.80$ are less than 1 when $\nu = 0.35$, it does not mean that the probabilities of the plunge and pitch motion escaping to the high-amplitude oscillation state are smaller than that when $\nu = 0.1$. In fact, larger $\nu$ increases the value of $N$ in $P_E = M/N$. While this intensity is not enough to make the increased local maxima exceed the unstable solution, the value of $M$ is hardly changed. Similarly, as shown in Figs. 6(c) and 6(d), as $A$ gradually approaches

**TABLE I.** The lengths of $R_{\xi-\Omega}$ and $R_{\alpha-\Omega}$ under different $\nu$.

| $\nu$ | $R_{\xi-\Omega}$ | $R_{\alpha-\Omega}$ |
|---|---|---|
| 0.1 | [0.80, 0.832] | [0.80, 0.830] |
| 0.35 | [0.80, 1.030] | [0.80, 0.852] |

**TABLE II.** The lengths of $R_{\xi-A}$ and $R_{\alpha-A}$ under different $\nu$.

| $\nu$ | $R_{\xi-A}$ | $R_{\alpha-A}$ |
|---|---|---|
| 0.1 | [1.667, 2.7] | [1.704, 2.7] |
| 0.35 | [0.932, 2.7] | [1.364, 2.7] |

01 April 2026 12:40:30


Published under an exclusive license by AIP Publishing

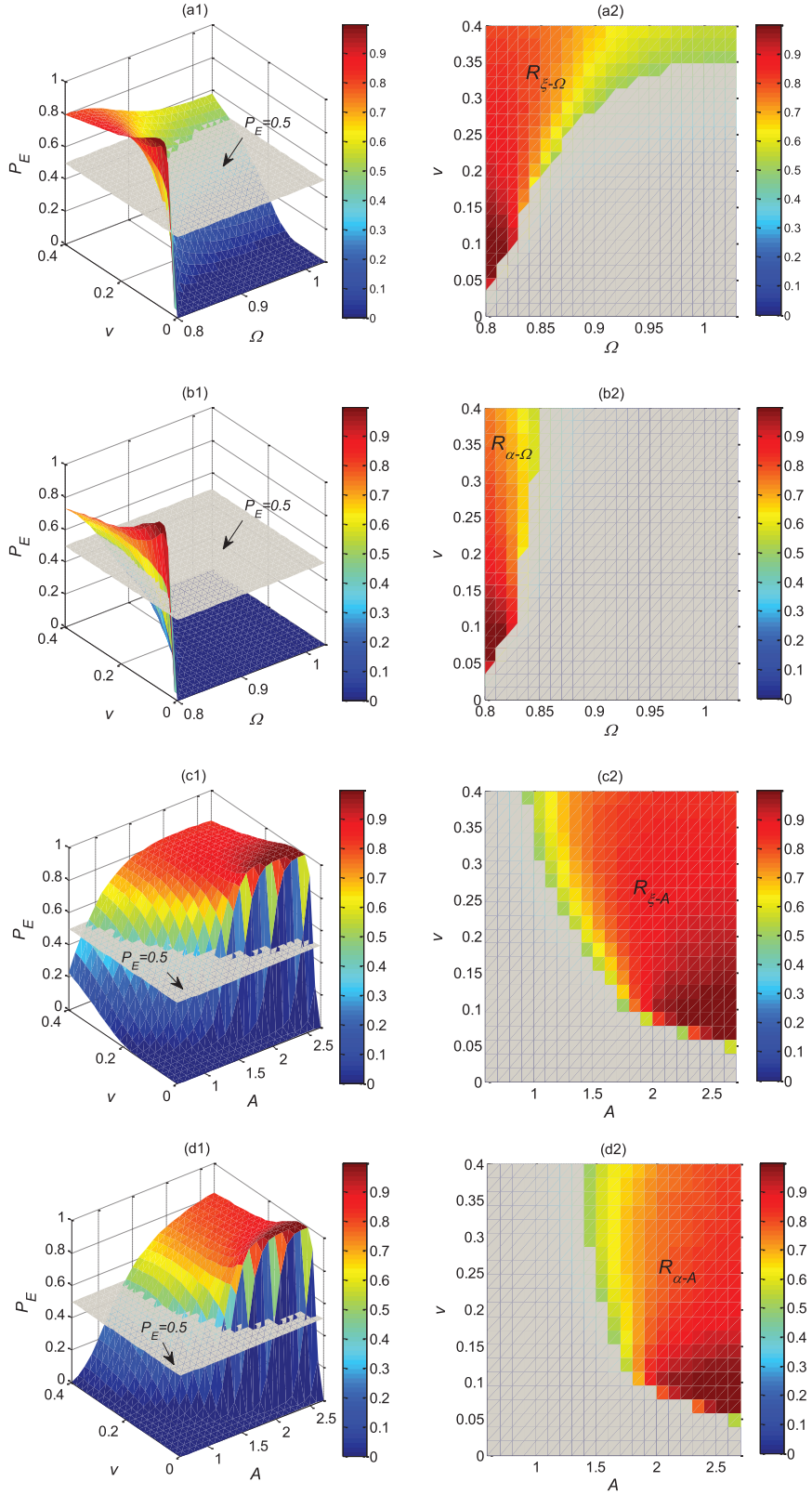


**FIG. 8.** The high-risk regions of noise-induced high-amplitude oscillations in the plunge and pitch motion. The inserted plane represents $P_E = 0.5$. (a) $R_{\xi-\Omega}$ under $\Omega$ vs $v$; (b) $R_{\alpha-\Omega}$ under $\Omega$ vs $v$; (c) $R_{\xi-A}$ under $A$ vs $v$; (d) $R_{\alpha-A}$ under $A$ vs $v$.

01 April 2026 12:40:30


Published under an exclusive license by AIP Publishing

the bifurcation point $A = 2.7$, the probabilities of the plunge and pitch motion escaping to the high-amplitude oscillation state also gradually increase.

After the escape probability is obtained, another important problem is to determine a critical value of $P_E$. Since we have not yet obtained a more precise critical value of $P_E$, we directly take $P_E = 0.5$ to approximately judge whether the noise-induced high-amplitude oscillations occur. Perhaps, there are more accurate results than 0.5, we will further explore it in future research. Then, a more general, early warning indicator of noise-induced catastrophic high-amplitude oscillations is defined as follows:

*Definition 1*. For the escape probability of the plunge or pitch motion under a fixed $v$ and $\Omega \in [0.80,\ 1.03]$, the set of $\Omega$ satisfying

$$P_E \geq 0.5$$

is defined as the *high-risk region* of noise-induced catastrophic high-amplitude oscillations in the plunge or pitch motion, which is correspondingly denoted as $R_{\xi-\Omega}$ or $R_{\alpha-\Omega}$.

Similarly, the high-risk region of the plunge or pitch motion at about $A \in [0.6, 2.7]$ can be defined below.

*Definition 2*. For the escape probability of plunge or pitch motion under a fixed $v$ and $A \in [0.6, 2.7]$, the set of $A$ satisfying

$$P_E \geq 0.5$$

is defined as the *high-risk region* of noise-induced catastrophic high-amplitude oscillations in the plunge or pitch motion, which is correspondingly denoted as $R_{\xi-A}$ or $R_{\alpha-A}$.

Based on Definition 1, $P_E$ and the corresponding $R_{\xi-\Omega}$ (thick bar-type) and $R_{\alpha-\Omega}$ (thin bar-type) under different $v$ are shown in Figs. 7(a) and 7(b). In addition, the lengths of $R_{\xi-\Omega}$ and $R_{\alpha-\Omega}$ with respect to different $v$ are presented in Table I. It is found that $R_{\xi-\Omega}$ and $R_{\alpha-\Omega}$ increase with increasing $v$. When $v = 0.35$, even the whole $\Omega \in [0.80,\ 1.03]$ becomes $R_{\xi-\Omega}$ as shown in Fig. 7(b). Similarly, based on Definition 2, $P_E$ and the corresponding $R_{\xi-A}$ (thick bar-type) and $R_{\alpha-A}$ (thin bar-type) under different $v$ are also shown in Figs. 7(c) and 7(d). The lengths of $R_{\xi-A}$ and $R_{\alpha-A}$ under different $v$ are also presented in Table II. Obviously, the noise intensity still plays a crucial role to expand the lengths of $R_{\xi-A}$ and $R_{\alpha-A}$: the larger $v$ is, the larger the ranges of $R_{\xi-A}$ and $R_{\alpha-A}$ are. These phenomena are also associated with earlier noise-induced high-amplitude oscillations that take place under strong fluctuations. Furthermore, it can be found from Fig. 7 that random fluctuations are more likely to induce high-amplitude oscillations in the plunge motion than in the pitch motion.

To be more intuitive, Fig. 8 shows the space diagrams of the high-risk regions with respect to different parameters of the random excitation. Obviously, as $v$ increases, either $R_{\xi-\Omega}$, $R_{\alpha-\Omega}$ or $R_{\xi-A}$, $R_{\alpha-A}$ increase. Moreover, as shown in Figs. 8(a2) and 8(b2), the closer $\Omega$ is to the bifurcation point $\Omega = 0.80$, the larger the ranges of the corresponding high-risk regions. Similar results also exist in Figs. 8(c2) and 8(d2), as $A$ approaches the bifurcation point $A = 2.7$. It means that noise-induced high-amplitude oscillations are more likely to take place in advance. Comparing Figs. 8(c1) and 8(c2) with Figs. 8(d1) and 8(d2), it is also found that the trends of $R_{\xi-A}$ and $R_{\alpha-A}$ are similar against $A$, while this does not happen in $R_{\xi-\Omega}$ and $R_{\alpha-\Omega}$ against $\Omega$. Nevertheless, once $\Omega$ and $v$ belong to $R_{\xi-\Omega}$ or $R_{\alpha-\Omega}$, and $A$ and $v$ belong to $R_{\xi-A}$ or $R_{\alpha-A}$, there is a high possibility that noise-induced high-amplitude oscillations are impending.

In the above results, $A = 1.5$ is taken in quantifying the high-risk regions of plunge and pitch motion under $\Omega$ vs $v$, and $\Omega = 0.84$ is taken in quantifying the high-risk regions of plunge and pitch motion under $A$ vs $v$. In fact, based on the introduced method here, more interesting phenomena can also be obtained for other $A$ or $\Omega$ values. As the well-known concept of basin stability, the quantified high-risk regions are the important geometric structures that can be used to predict noise-induced catastrophic high-amplitude oscillations in engineering systems.

## V. CONCLUSIONS

In this paper, we have focused on a TDOFA model with an external random loading as a concrete example to detect the tipping from a low-amplitude oscillation state to a high-amplitude one. First of all, the approximate analytical solutions of the amplitude–frequency responses obtained by the multiple-scale method are compared with the results from Monte Carlo numerical simulations. It provides a correct guarantee for us to directly use the numerical method to warn noise-induced catastrophic high-amplitude oscillations. Then, the influences of different parameters of the random excitation on the amplitude responses are discussed in detail. Among them, noise-induced high-amplitude oscillations that take place earlier are uncovered. Based on the escape probability, finally, the concept of the high-risk region is introduced. It provides early warning signals via quantifying the ranges of the parameters where noise-induced catastrophic high-amplitude oscillations may occur. Once the central frequency $\Omega$, the amplitude $A$, and the noise intensity $v$ enter the quantified high-risk regions, there is a high possibility that noise-induced catastrophic high-amplitude oscillations are impending. Now, some performance should be designed to avert them.

However, in the definitions of the high-risk regions, the scale factor is taken as $P_E = 1/2$. More accurate results may be realized in terms of other values, which need to be further explored. Furthermore, it should be noted that only additive random noisy fluctuations are considered here to study the noise-induced critical jumps in an airfoil model. Owing to the complexity of quasi- or unsteady aerodynamics, achieving the quantification of high-risk regions of catastrophic high-amplitude oscillations with more complex random fluctuations is worth further investigation. Although the high-risk region of noise-induced catastrophic high-amplitude oscillations is established based on a simple random airfoil model, our work may provide some new ideas for the early warning of catastrophic high-amplitude oscillations in real airfoil systems and even may provide some valuable perspectives for aircraft designers to avoid the occurrence of catastrophic high-amplitude oscillations. More importantly, our work may be extended to the early warnings of other practical engineering systems, such as thermoacoustic systems and rotor-bearing systems.

## ACKNOWLEDGMENTS

This paper was supported by the National Natural Science Foundation of China under Grant Nos. 12102237 and 12072264,

01 April 2026 12:40:30


Published under an exclusive license by AIP Publishing

the Key International (Regional) Joint Research Program of the National Natural Science Foundation of China under Grant No. 12120101002, the Natural Science Foundation of Shanxi Province under Grant No. 20210302124387, the Research Funds for Interdisciplinary Subject of Northwestern Polytechnical University, and the Shaanxi Provincial Key R&D Program (Nos. 2020KW-013 and 2019TD-010).

## AUTHOR DECLARATIONS

### Conflict of Interest

The authors have no conflicts to disclose.

## DATA AVAILABILITY

Data sharing is not applicable to this article as no new data were created or analyzed in this study.

## APPENDIX: STEADY-STATE AMPLITUDE–FREQUENCY RESPONSE

The multiple-scale method is applied only for the primary resonance, i.e., the excitation frequency is close to the natural frequency of the airfoil model. Then, system (2) can be rewritten as[45,46]

$$\begin{aligned}\ddot{\xi}+\varepsilon x_\alpha\ddot{\alpha}+\varepsilon\zeta_\xi\dot{\xi}+\Omega^2x_1-\varepsilon\sigma_1x_1+\varepsilon{\omega_{10}}^2\beta_\xi\xi^3&=-2\varepsilon Q\alpha/\mu,\\ \varepsilon\frac{x_\alpha}{{r_\alpha}^2}\ddot{\xi}+\ddot{\alpha}+\varepsilon\zeta_\alpha\dot{\alpha}+\Omega^2x_2-\varepsilon\sigma_2x_2+\varepsilon\beta_\alpha\alpha^3&\\ =\varepsilon A\cos[\Omega t+\nu W(\tau)],&\end{aligned}\tag{A1}$$

in which, $\Omega^2={\omega_{10}}^2+\varepsilon\sigma_1$ and $\Omega^2={\omega_{20}}^2+\varepsilon\sigma_2$. $\sigma_1$ and $\sigma_2$ are the detuning parameters of plunge and pitch motion, respectively.

First of all, the fast and slow time scales are introduced as follows:

$$T_0=\tau,\quad T_1=\varepsilon,\quad T_2=\varepsilon^2\tau,\quad \ldots,$$

Then, using the differential operators

$$D_0=\frac{\partial}{\partial T_0},\quad D_1=\frac{\partial}{\partial T_1},\quad D_2=\frac{\partial}{\partial T_2},\quad \ldots,$$

and the chain rule, the ordinary time derivatives can be transformed into partial derivatives as

$$\frac{d}{d\tau}=D_0+\varepsilon D_1+\varepsilon^2D_2+\cdots,$$

$$\frac{d^2}{d\tau^2}=D_0^2+2\varepsilon D_0D_1+\varepsilon^2(D_1^2+2D_0D_2)+\cdots.$$

According to the standard procedure of the multiple-scale method, we look for the uniformly approximate solutions of system (A1) in the form

$$\begin{aligned}\xi&=\xi_{10}(T_0,T_1)+\varepsilon\xi_{11}(T_0,T_1)+\cdots,\\ \alpha&=\alpha_{20}(T_0,T_1)+\varepsilon\alpha_{21}(T_0,T_1)+\cdots.\end{aligned}\tag{A2}$$

Substituting Eq. (A2) into system (A1), and separating terms based on the power of $\varepsilon$, we have the following:

Order $\varepsilon^0$:

$$\begin{cases}D_0^2\xi_{10}+\Omega^2\xi_{10}=0,\\ D_0^2\alpha_{20}+\Omega^2\alpha_{20}=0.\end{cases}\tag{A3}$$

Order $\varepsilon^1$:

$$\begin{cases}D_0^2\xi_{11}+\Omega^2\xi_{11}=-2D_0D_1\xi_{10}-x_\alpha D_0^2\alpha_{20}-\zeta_\xi D_0\xi_{10}+\sigma_1\xi_{10}-{\omega_{10}}^2\beta_\xi{\xi_{10}}^3-2Q\alpha_{20}/\mu,\\ D_0^2\alpha_{21}+\Omega^2\alpha_{21}=-2D_0D_1\alpha_{20}-\frac{x_\alpha}{{r_\alpha}^2}D_0^2\xi_{10}-\zeta_\alpha D_0\alpha_{20}+\sigma_2\alpha_{20}-\beta_\alpha{\alpha_{20}}^3+A\cos[\Omega t+\nu W(\tau)].\end{cases}\tag{A4}$$

The general solutions of Eq. (A3) can be obtained as

$$\begin{cases}\xi_{10}=A_1(T_1)e^{i\Omega T_0}+c.c.,\\ \alpha_{20}=A_2(T_1)e^{i\Omega T_0}+c.c.,\end{cases}\tag{A5}$$

Here, *c.c.* denotes the complex conjugate of the preceding terms [i.e., $\overline{A_1}(T_1)e^{-i\Omega T_0}$]. Substituting Eq. (A5) into Eq. (A4), we obtain

$$\begin{cases}D_0^2\xi_{11}+\Omega^2\xi_{11}=(-2i\Omega D_1A_1+x_\alpha\Omega^2A_2-i\zeta_\xi\Omega A_1+\sigma_1A_1-3{\omega_{10}}^2\beta_\xi A_1^2\overline{A_1}-2Q/\mu A_2)e^{i\Omega T_0}-{\omega_{10}}^2\beta_\xi A_1^3e^{3i\Omega T_0}+c.c.,\\ D_0^2\alpha_{21}+\Omega^2\alpha_{21}=(-2i\Omega D_1A_2+\frac{x_\alpha}{{r_\alpha}^2}\Omega^2A_1-i\zeta_\alpha\Omega A_2+\sigma_2A_2-3\beta_\alpha A_2^2\overline{A_2}+\frac{1}{2}fe^{i\bar{\nu}W(T_1)})e^{i\Omega T_0}-\beta_\alpha A_2^3e^{3i\Omega T_0}+c.c.,\end{cases}\tag{A6}$$

where $\overline{A_i}$, $i=1,2$ denote the conjugate of $A_i$, $D_1A_i$, $i=1,2$ are the derivative with the respect to the slow time scale $T_1$, and

$$\nu W(\tau)=\nu W(T_0)=\nu W\left(\frac{T_1}{\varepsilon}\right)=\frac{\nu}{\sqrt{\varepsilon}}W(T_1):=\bar{\nu}W(T_1).$$

Eliminating the secular terms in Eq. (A6), one obtains

$$\begin{cases}-2i\Omega D_1A_1+x_\alpha\Omega^2A_2-i\zeta_\xi\Omega A_1+\sigma_1A_1-3{\omega_{10}}^2\beta_\xi A_1^2\overline{A_1}-2Q/\mu A_2=0,\\ -2i\Omega D_1A_2+\frac{x_\alpha}{{r_\alpha}^2}\Omega^2A_1-i\zeta_\alpha\Omega A_2+\sigma_2A_2-3\beta_\alpha A_2^2\overline{A_2}+\frac{1}{2}Ae^{i\bar{\nu}W(T_1)}=0.\end{cases}\tag{A7}$$

01 April 2026 12:40:30


Published under an exclusive license by AIP Publishing

Then, substituting $A_1(T_1) = \frac{1}{2}a_1(T_1)e^{i\varphi_1(T_1)}$ $\left(\overline{A_1}(T_1) = \frac{1}{2}a_1(T_1)e^{-i\varphi_1(T_1)}\right)$, $A_2(T_1) = \frac{1}{2}a_2(T_1)e^{i\varphi_2(T_1)}$ $\left(\overline{A_2}(T_1) = \frac{1}{2}a_2(T_1)e^{-i\varphi_2(T_1)}\right)$ into Eq. (A7), and separating the real and imaginary parts, one arrives at

$$\begin{cases} D_1 a_1 = -\frac{1}{2\Omega}\zeta_\xi a_1 + \frac{1}{2\Omega}(x_\alpha\Omega^2 - 2Q/\mu)a_2\sin\theta_1, \\ a_1 D_1\varphi_1 = -\frac{1}{2\Omega}\sigma_1 a_1 + \frac{3}{8\Omega}{\omega_{10}}^2\beta_\xi a_1^3 - \frac{1}{2\Omega}(x_\alpha\Omega^2 - 2Q/\mu)a_2\cos\theta_1, \\ D_1 a_2 = -\frac{1}{2}\zeta_\alpha a_2 - \frac{1}{2}\frac{x_\alpha}{{r_\alpha}^2}\Omega a_1\sin\theta_1 + \frac{A}{2\Omega}\sin\theta_2, \\ a_2 D_1\varphi_2 = -\frac{1}{2\Omega}\sigma_2 a_2 + \frac{3}{8\Omega}\beta_\alpha a_2^3 - \frac{1}{2}\frac{x_\alpha}{{r_\alpha}^2}\Omega a_1\cos\theta_1 - \frac{A}{2\Omega}\cos\theta_2, \end{cases} \tag{A8}$$

where $\theta_1 = \varphi_2 - \varphi_1$, $\theta_2 = \bar{\nu}W(T_1) - \varphi_2$.

Here, we are mainly interested in the steady-state responses of system (A1) in the deterministic case ($\nu = 0$), which lays a solid foundation for us to directly use the numerical method to study noise-induced high-amplitude oscillations. Hence, $D_1 a_1 = D_1 a_2 = 0$ and $D_1\theta_1 = D_1\theta_2 = 0$ need to be considered. According to Eq. (A8), we get

$$\begin{cases} -\frac{1}{2}\zeta_\xi a_1 + \frac{1}{2\Omega}(x_\alpha\Omega^2 - 2Q/\mu)a_2\sin\theta_1 = 0, \\ -\frac{1}{2\Omega}\sigma_1 a_1 + \frac{3}{8\Omega}{\omega_{10}}^2\beta_\xi a_1^3 - \frac{1}{2\Omega}(x_\alpha\Omega^2 - 2Q/\mu)a_2\cos\theta_1 = 0, \\ -\frac{1}{2}\zeta_\alpha a_2 + \frac{1}{2}\frac{x_\alpha}{{r_\alpha}^2}\Omega a_1\sin\theta_1 + \frac{A}{2\Omega}\sin\theta_2 = 0, \\ -\frac{1}{2\Omega}\sigma_2 a_2 + \frac{3}{8\Omega}\beta_\alpha a_2^3 - \frac{1}{2}\frac{x_\alpha}{{r_\alpha}^2}\Omega a_1\cos\theta_1 - \frac{A}{2\Omega}\cos\theta_2 = 0. \end{cases} \tag{A9}$$

By eliminating the parameters $\theta_1$ and $\theta_2$ in Eq. (A9), one can derive the following steady-state amplitude–frequency relations

$$\begin{cases} \left(\frac{\Omega\mu\zeta_\xi a_1}{a_0(\mu x_\alpha\Omega^2 - 2Q)}\right)^2 + \left(\frac{3\mu{\omega_{10}}^2\beta_\xi a_1^3}{4a_2(\mu x_\alpha\Omega^2 - 2Q)} - \frac{\mu\sigma_1 a_1}{a_2(\mu x_\alpha\Omega^2 - 2Q)}\right)^2 = 1, \\ \left(\Omega\zeta_\alpha a_2 + \frac{x_\alpha\Omega^3 a_1^2\mu\zeta_\xi}{{r_\alpha}^2 a_2(\mu x_\alpha\Omega^2 - 2Q)}\right)^2 + \left(\frac{3}{4}\beta_\alpha a_2^3 - \sigma_2 a_2 - \frac{3x_\alpha\Omega^2\mu{\omega_{10}}^2\beta_\xi a_1^4}{{r_\alpha}^2 4a_2(\mu x_\alpha\Omega^2 - 2Q)} - \frac{x_\alpha\Omega^2 a_1^2\mu\sigma_1}{{r_\alpha}^2 a_2(\mu x_\alpha\Omega^2 - 2Q)}\right)^2 = A^2. \end{cases} \tag{A10}$$

By solving Eq. (A10), $a_1$ and $a_2$ can be obtained, and the steady-state amplitude–frequency response of plunge and pitch motion can be explored.

## REFERENCES


[1] E. A. Gopalakrishnan, Y. Sharma, T. John, P. S. Dutta, and R. I. Sujith, "Early warning signals for critical transitions in a thermoacoustic system," Sci. Rep. **6**, 35310 (2016).
[2] X. Zhang, Y. Xu, Q. Liu, J. Kurths, and C. Grebogi, "Rate-dependent tipping and early warning in a thermoacoustic system under extreme operating environment," Chaos **31**, 113115 (2021).
[3] B. H. K. Lee, S. J. Price, and Y. S. Wong, "Nonlinear aeroelastic analysis of airfoils: Bifurcation and chaos," Prog. Aerosp. Sci. **35**, 205–334 (1999).
[4] F. X. Chen, Y. M. Chen, and J. K. Liu, "Equivalent linearization method for the flutter system of an airfoil with multiple nonlinearities," Commun. Nonlinear Sci. Numer. Simul. **17**, 4529–4535 (2012).
[5] G. Han, Y. Chen, and X. Wang, "Flutter analysis of bending-torsion coupling of aero-engine compressor blade with assembled clearance," Appl. Math. Modell. **39**, 2539–2553 (2015).
[6] R. Vasconcellos, A. Abdelkefi, M. R. Hajj, and F. D. Marques, "Grazing bifurcation in aeroelastic systems with freeplay nonlinearity," Commun. Nonlinear Sci. Numer. Simul. **19**, 1611–1625 (2014).
[7] E. Verstraelen, G. Dimitriadis, G. D. B. Rossetto, and E. H. Dowell, "Two-domain and three-domain limit cycles in a typical aeroelastic system with freeplay in pitch," J. Fluids Struct. **69**, 89–107 (2017).
[8] Z. Monfared, Z. Afsharnezhad, and J. A. Esfahani, "Flutter, limit cycle oscillation, bifurcation and stability regions of an airfoil with discontinuous freeplay nonlinearity," Nonlinear Dyn. **90**, 1965–1986 (2017).
[9] G. Liu, L. Wang, J. K. Liu, Y. M. Chen, and Z. R. Lu, "Identification of an airfoil-store system with cubic nonlinearity via enhanced response sensitivity approach," AIAA J. **56**, 4977–4987 (2018).
[10] Q. Liu, Y. Xu, and J. Kurths, "Active vibration suppression of a novel airfoil model with fractional order viscoelastic constitutive relationship," J. Sound Vibr. **432**, 50–64 (2018).
[11] C. L. Pettit, "Uncertainty quantification in aeroelasticity: Recent results and research challenges," J. Aircraft **41**, 1217–1229 (2004).
[12] R. X. Mei, Y. Xu, Y. G. Li, and J. Kurths, "Characterizing stochastic resonance in a triple cavity," Philos. Trans. R. Soc. A **379**, 20200230 (2020).
[13] X. Y. Zhang, Y. Xu, Q. Liu, and J. Kurths, "Rate-dependent tipping-delay phenomenon in a thermoacoustic system with colored noise," Sci. Chin. Technol. Sci. **63**, 2315–2327 (2020).
[14] Y. Huang and G. Tao, "A feedback control strategy for the airfoil system under non-Gaussian colored noise excitation," Chaos **24**, 033117 (2014).
[15] Y. Xu, Q. Liu, G. Guo, C. Xu, and D. Liu, "Dynamical responses of airfoil models with harmonic excitation under uncertain disturbance," Nonlinear Dyn. **89**, 1579–1590 (2017).
[16] Q. Liu, Y. Xu, C. Xu, and J. Kurths, "The sliding mode control for an airfoil system driven by harmonic and colored Gaussian noise excitations," Appl. Math. Modell. **64**, 249–264 (2018).
[17] R. V. Bethi, S. V. Gali, and J. Venkatramani, "Response analysis of a pitch–plunge airfoil with structural and aerodynamic nonlinearities subjected to randomly fluctuating flows," J. Fluids Struct. **92**, 102820 (2020).
[18] D. C. Poirel and S. J. Price, "Post-instability behavior of a structurally nonlinear airfoil in longitudinal turbulence," J. Aircr. **34**, 619–626 (1997).
[19] P. Singh, H. C. Yeong, H. Zhang, Z. Rapti, and N. S. Namachchivaya, "Stochastic stability and dynamics of a two-dimensional structurally nonlinear airfoil in turbulent flow," Meccanica **51**, 2665–2688 (2016).
[20] S. Sazesh and S. Shams, "Nonlinear aeroelastic analysis of an airfoil with control surface free-play using stochastic approach," J. Fluids Struct. **72**, 114–126 (2017).
[21] Q. Liu, Y. Xu, Y. Li, J. Kurths, and X. Liu, "Fixed-interval smoothing of an aeroelastic airfoil model with cubic or free-play nonlinearity in incompressible flow," Acta Mech. Sin. **37**, 1168 (2021).
[22] P. J. Attar and P. Vedula, "Direct quadrature method of moments solution of Fokker-Planck equations in aeroelasticity," AIAA J. **47**, 1219–1227 (2009).


01 April 2026 12:40:30


Published under an exclusive license by AIP Publishing

[23]J. Venkatramani, V. Nair, R. I. Sujith, S. Gupta, and S. Sarkar, "Multi-fractality in aeroelastic response as a precursor to flutter," J. Sound Vibr. **386**, 390–406 (2017).
[24]J. Venkatramani, S. Sarkar, and S. Gupta, "Investigations on precursor measures for aeroelastic flutter," J. Sound Vibr. **419**, 318–336 (2018).
[25]J. Venkatramani, S. Sarkar, and S. Gupta, "Intermittency in pitch-plunge aeroelastic systems explained through stochastic bifurcations," Nonlinear Dyn. **92**, 1225–1241 (2018).
[26]D. C. Poirel and S. J. Price, "Structurally nonlinear fluttering airfoil in turbulent flow," AIAA J. **39**, 1960–1968 (2001).
[27]D. C. Poirel and S. J. Price, "Random binary (coalescence) flutter of a two-dimensional linear airfoil," J. Fluids Struct. **18**, 23–42 (2003).
[28]W. Q. Zhu and G. Q. Cai, "Random vibration of viscoelastic system under broad-band excitations," Int. J. Non-Linear Mech. **46**, 720–726 (2011).
[29]J. Deng, "Higher-order stochastic averaging for a SDOF fractional viscoelastic system under bounded noise excitation," J. Franklin Inst. **354**, 7917–7945 (2017).
[30]T. Nakano, N. Fujisawa, and S. Lee, "Measurement of tonal-noise characteristics and periodic flow structure around NACA0018 airfoil," Exp. Fluids **40**, 482–490 (2006).
[31]E. C. Nash, M. V. Lowson, and A. Mcalpine, "Boundary-layer instability noise on aerofoils," J. Fluid Mech. **382**, 27–61 (1999).
[32]B. Plogmann, A. Herrig, and W. Würz, "Experimental investigations of a trailing edge noise feedback mechanism on a NACA 0012 airfoil," Exp. Fluids **54**, 1480 (2013).
[33]S. Takagi and Y. Konishi, "Frequency selection mechanism of airfoil trailing-edge noise," J. Aircr. **47**, 1111–1116 (2010).
[34]R. E. Longhouse, "Vortex shedding noise of low tip speed, axial flow fans," J. Sound Vibr. **53**, 25–46 (1977).
[35]T. P. Chong and P. F. Joseph, "An experimental study of airfoil instability tonal noise with trailing edge serrations," J. Sound Vibr. **332**, 6335–6358 (2013).
[36]Q. Liu, Y. Xu, and J. Kurths, "Bistability and stochastic jumps in an airfoil system with viscoelastic material property and random fluctuations," Commun. Nonlinear Sci. Numer. Simul. **84**, 105184 (2020).
[37]J. Ma, Y. Xu, Y. Li, R. Tian, and J. Kurths, "Predicting noise-induced critical transitions in bistable systems," Chaos **29**, 081102 (2019).
[38]J. Ma, Y. Xu, Y. Li, R. Tian, G. Chen, and J. Kurths, "Precursor criteria for noise-induced critical transitions in multi-stable systems," Nonlinear Dyn. **101**, 21–35 (2020).
[39]J. Ma, Y. Xu, Y. Li, R. Tian, S. Ma, and J. Kurths, "Quantifying the parameter dependent basin of the unsafe regime of asymmetric Lévy-noise-induced critical transitions," Appl. Math. Mech. **42**, 65–84 (2021).
[40]J. Z. Ma, Y. Xu, W. Xu, Y. G. Li, and J. Kurths, "Slowing down critical transitions via Gaussian white noise and periodic force," Sci. Chin. Technol. Sci. **62**, 2144–2152 (2019).
[41]Y. Li, R. Mei, Y. Xu, J. Kurths, J. Duan, and R. Metzler, "Particle dynamics and transport enhancement in a confined channel with position-dependent diffusivity," New J. Phys. **22**, 053016 (2020).
[42]W. Zan, Y. Xu, R. Metzler, and J. Kurths, "First-passage problem for stochastic differential equations with combined parametric Gaussian and Lévy white noises via path integral method," J. Comput. Phys. **435**, 110264 (2021).
[43]Y. Zhang, Y. Jin, and Y. Li, "Enhanced energy harvesting using time-delayed feedback control from random rotational environment," Physica D **422**, 132908 (2021).
[44]J. Ma, Y. Xu, D. Liu, R. Tian, S. Ma, U. Feudel, and J. Kurths, "Suppression of noise-induced critical transitions: A linear augmentation method," Eur. Phys. J. Spec. Top. **230**, 3281–3290 (2021).
[45]A. H. Nayfeh, *Perturbation Methods* (John Wiley, New York, 1973).
[46]Y. Xu, Y. Li, and D. Liu, "A method to stochastic dynamical systems with strong nonlinearity and fractional damping," Nonlinear Dyn. **83**, 2311–2321 (2016).

01 April 2026 12:40:30


Published under an exclusive license by AIP Publishing